The Report Committee for Andrew Jay Erickson

Certifies that this is the approved version of the following report:

Simulation of the Growth of Multiple Interacting

2D Hydraulic Fractures Driven by an Inviscid Fluid

APPROVED BY

SUPERVISING COMMITTEE:

Supervisor: _____

Mark E. Mear

_____

Chad M. Landis

Simulation of the Growth of Multiple Interacting 2D Hydraulic Fractures Driven by an Inviscid Fluid

by

Andrew Jay Erickson, B.A.

Report

Presented to the Faculty of the Graduate School

of The University of Texas at Austin

in Partial Fulfillment

of the Requirements

for the Degree of

Master of Science in Engineering

The University of Texas at Austin

December 2012

Dedicated to my family.

ACKNOWLEDGMENTS

I wish to thank my advisor, Professor Mark E. Mear, for his advice, guidance, and support during this research and over the course of my studies at The University of Texas at Austin. I would also like to thank Professor Chad M. Landis, for providing suggestions and comments, but also for his support and understanding thoughout my program of work. Additionally, I would like to thank Conoco-Phillips, Dr. Rick Dean, and Dr. Joseph Schmidt for their financial support and technical guidance over the course of this investigation. Finally, I would like to thank Linnea, my friends, and my family for all of their love and support.

Simulation of the Growth of Multiple Interacting

2D Hydraulic Fractures Driven by an Inviscid Fluid

by

Andrew Jay Erickson, M.S.E.

The University of Texas at Austin, 2012

SUPERVISOR: Mark E. Mear

In this paper we develop a computational procedure to investigate linear fracture of two-dimensional problems in isotropic linearly elastic media. A symmetric Galerkin boundary element method (SGBEM), based on a weakly singular, weak-form traction integral equation, is adopted to model these fractures. In particular we consider multiple interacting cracks in an unbounded domain subject to internal pressure and remote stress. The growth of the cracks is driven by either linearly dependent injection pressures or volumes in each crack. A variety of crack geometries are investigated.

TABLE OF CONTENTS

LIST OF TABLES

LIST OF FIGURES

CHAPTER 1
INTRODUCTION

In this paper a computational procedure is developed to investigate linear fracture analysis of two-dimensional problems in isotropic elastic media as a simple model of hydraulic fracturing in natural gas wells. We present a procedure to model the growth multiple cracks in an unbounded domain and calculate the minimum injection pressure or volume necessary to propagate the cracks. We first present the computational procedure and solution strategy utilized in our boundary element method code, which we will call HyFrac2D. Several well known stress intensity factor solutions are then utilized to verify the accuracy of of numerical techniques. Next, we investigate the growth of a variety of crack geometries subject to either equal injection pressures or equal injection volumes. Finally, for the case of equal injection volumes in parallel cracks, we then investigate what we will term "antisymmetric" behavior.

CHAPTER 2
MATHEMATICAL PRELIMINARIES

2.1 Governing Equation for Fractures

Our computational procedure relies upon a singularity-reduced integral relation, derived by Han Tran, giving the traction t_k acting at a point on the crack surface, $\mathbf{y} \in \Gamma_c$, as

$$t_k(\mathbf{y}) = D\bigg[\int_{\Gamma_c} C_j^k(\boldsymbol{\xi} - \mathbf{y})\, D\Delta u_j(\boldsymbol{\xi}) ds(\boldsymbol{\xi})\bigg],$$

in which $D = \partial/\partial s$ denotes the derivative with respect to arc length along the crack line, Δu_j is the relative crack-face displacement, and C_j^k is a weakly singular kernel given below (Tran 2010).

A regularized weak-form traction integral equation for the traction applied at a point on the crack surface is then obtained by multiplying both sides of the traction equation by a continuous test function $\Delta\tilde{u}_k(\mathbf{y})$ (that has the property $\Delta\tilde{u}_k = 0$ at the crack tips). Integrating the result over Γ_c and finally integrating by parts yields

$$\int_{\Gamma_c} t_k(\mathbf{y})\, \Delta\tilde{u}_k(\mathbf{y})\, ds(\mathbf{y}) = -\int_{\Gamma_c} D\Delta\tilde{u}_k(\mathbf{y}) \int_{\Gamma_c} C_j^k(\boldsymbol{\xi} - \mathbf{y})\, D\Delta u_j(\boldsymbol{\xi})\, ds(\boldsymbol{\xi})\, ds(\mathbf{y}).$$

Though an expressions for the kernel C_j^k applicable to general anisotropy was obtained by Han Tran, this formulation only utilizes the form of the kernel applicable to isotropic elastic materials, which is given by

$$\begin{aligned} C_\beta^\alpha(\boldsymbol{\xi} - \mathbf{y}) &= \tfrac{E}{4\pi(1-\nu^2)}\big[\ln\big(r/2\big)\delta_{\alpha\beta} + \tfrac{\delta_{\alpha\beta}}{2} - \tfrac{\partial r}{\partial \xi_\alpha}\tfrac{\partial r}{\partial \xi_\beta}\big] \\ C_3^3(\boldsymbol{\xi} - \mathbf{y}) &= \tfrac{E}{4\pi(1+\nu)}\ln\big(r/2\big). \end{aligned}$$

where $r = |\boldsymbol{\xi} - \mathbf{y}|$. Note that C_j^k is weakly-singular at $\boldsymbol{\xi} = \mathbf{y}$ in that it is order $\mathcal{O}(\ln r)$ as $r \to 0$.

We remark that the traction integral equation given above applies for an isolated crack. However, it is straightforward to generalize the integral equation to account for any (finite) number of interacting cracks, and this generalization is actually what is used in the scheme employed here.

2.2 Crack Tip Elements and Shape Functions

In order to numerically evaluate the system of traction integral equations, a Galerkin approach is adopted. Because the traction equation has a weakly-singular kernel, it is sufficient to use C^0 elements, and here we utilize standard quadratic isoparametric elements everywhere except for the crack tip elements. For crack tip elements, special shape functions are used to more accurately model the behavior of the crack opening displacements. As is well known, the relative crack-face displacement in in the vicinity of the crack tip has a square-root behavior. The special shape functions are defined on the master element associated with the crack tip element as shown in Figure 2.1.

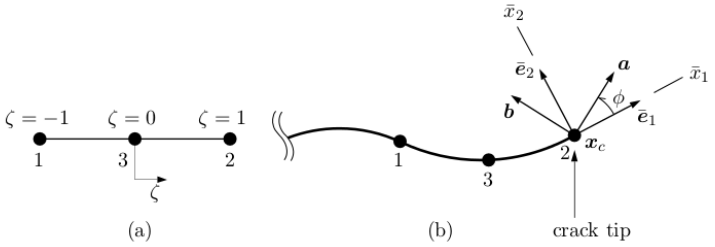

Figure 2.1: Master Element (a) and Crack Tip Element (b)

(Tran 2010)

Our special shape functions, $\psi_i'(\zeta)$, are given by

$$\psi_i'(\zeta) = \frac{\sqrt{1-\zeta}}{A_i(\zeta)}\psi_i(\zeta) \qquad \text{(no sum on i)}$$

where $\psi_i(\zeta)$ are the standard 3-node quadratic shape functions associated with the i^{th} node, and

$$A_i(\zeta) = \begin{cases} \sqrt{1-\zeta_i} & \text{for} \quad \zeta_i \neq 1 \\ \frac{1}{2} & \text{for} \quad \zeta_i = 1 \end{cases} \tag{2.1}$$

in which ζ_i is the coordinate on the master element of the i^{th} node. In the above formulation, $\psi = 1$ is associated with the crack tip node. For the case that $\psi = -1$ is the crack tip node, the expressions for ψ_i' and A_i are analogous, but simply have the $1-\zeta$ terms replaced with $1+\zeta$. The opening displacements on the crack tip element can be interpolated as

$$\Delta\mathbf{u} = \sqrt{1-\zeta}\sum_{i=1}^{3}\frac{\mathbf{u}_i}{A_i}\psi_i(\zeta)$$

where $\mathbf{u}_i$ are the unknown relative crack-face displacements of the i^{th} node *except* for the crack tip node where this quantity is actually directly related to the stress intensity factors; the stress intensity factors are, in essence, computed directly as part of the solution vector thus avoiding the need for post processing (see (Tran 2010) for additional details).

2.3 Crack Growth Criteria

The direction of crack growth is taken to be governed by the maximum hoop stress criterion. Consider our crack tip coordinate system shown in Figure 2.2. Axis 1 is in the tangential direction of the crack surface and directs into the material. Axis 2 is normal to axis 1 and directs in the opposite direction of the normal vector of the positive crack face, Γ_c^+, which is defined by the order of nodes of crack elements. We also note that σ_θ is the normal, or hoop, stress and $\mathbf{n}$ is the unit normal vector in the θ-direction.

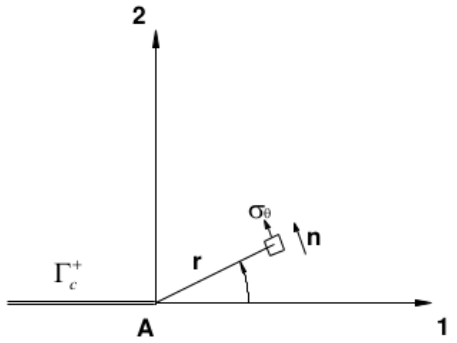

Figure 2.2: Crack Tip Coordinate System

(Tran 2010)

Let Δa denote the crack advance at a given crack tip and let θ_g be the angle of growth. The growth direction is then (according to the maximum hoop stress criterion) given by

$$\tan\left(\frac{\theta_g}{2}\right) = \frac{K_I - \sqrt{K_I^2 + 8K_{II}^2}}{4K_{II}}, \qquad -\pi \leq \theta_g \leq \pi$$

where K_I and K_{II} are the mode-I and mode-II stress intensity factors, respectively (Tran 2010). The amount of (relative) growth of each crack tip is taken to be governed by the following bi-linear growth law (which can be viewed as type of regularization of the growth law governing "ideally brittle" crack growth)

$$\frac{\Delta a}{\Delta a_0} = \begin{cases} 0 & , \quad \frac{\bar{K}_I}{K_{IC}} < 1-\beta \\ \frac{1-\alpha}{\beta-\alpha}\left(\frac{\bar{K}_I}{K_{IC}} - 1 + \beta\right) & , \quad 1-\beta \leq \frac{\bar{K}_I}{K_{IC}} < 1-\alpha \\ \frac{\bar{K}_I}{K_{IC}} & , \quad 1-\alpha \leq \frac{\bar{K}_I}{K_{IC}} \end{cases} \tag{2.2}$$

where $\bar{K}_I$ is an equivalent mode-I stress intensity factor defined by

$$\bar{K}_I = K_I \cos^3\left(\frac{\theta_g}{2}\right) - \frac{3}{2} K_{II} \cos\left(\frac{\theta_g}{2}\right) \sin\theta_g,$$

in which K_{IC} is the fracture toughness, and $\{\Delta a_0, \alpha, \beta\}$ are user-defined model constants. To prevent computational error when $\bar{K}_I$ at a given tip is very close to K_{IC}, we also require an additional user-defined parameter ε such that

$$1 - \varepsilon \leq \frac{\bar{K}_I}{K_{IC}} \leq 1 \Rightarrow \frac{\Delta a}{\Delta a_0} = 1$$

The bi-linear crack growth law can be visualized in Figure 2.3.

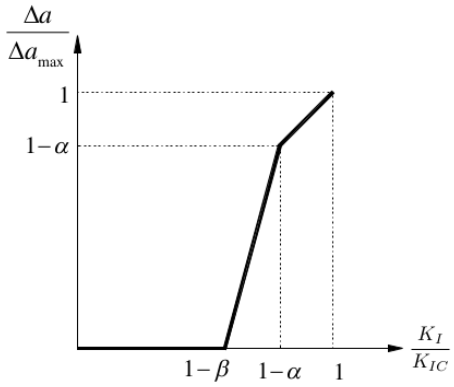

Figure 2.3: Bi-linear Crack Growth Law

(Han D. Tran and M.E. Mear 2010)

For each load step, $\bar{K}_I$ at each crack tip must not exceed K_{IC} and thus we scale our solution such that the maximum $\bar{K}_I$ is equal to K_{IC}. Thus, Δa_0 serves as the propagation step size for the crack tip with the largest hoop stress, accordingly the advance of the other crack tips is proportional to the ratio of it's equivalent mode-I stress intensity factor to the maximum hoop stress, which is to say the fracture toughness.

2.4 Solution Strategy

We explore two different scenarios for the propagation of multiple interacting hydraulic fractures; in both cases the fluid within the crack is idealized as being inviscid so that the pressure within the crack is uniform. We consider n cracks in an elastic media subject to an

anisotropic remote stress and either equal internal pressure (for all the cracks) or equal fluid volume injection (for all the cracks). Towards modeling the crack propagation, the solution algorithm first uses the solution for a unit pressure (prescribed individually in each crack) as a means to find the crack tip for which the stress intensity factor first reaches the critical SIF, which is to say $\bar{K}_I = K_{IC}$. We scale the unit pressure to find the pressure at which this tip first begins to grow. The code scales the pressure in each crack and the volumes of each crack accordingly to investigate crack growth as a function of either injection pressure or injection volume.

2.4.1 Linearly Dependent Injection Pressures

We first consider a strategy to simulate crack propagation due to linearly dependent injection pressures. HyFrac2D computes the pressure scaling, α_j^P, necessary to propagate the cracks at each load step. These pressure scaling values are subject to the following stress intensity factor constraint:

$$K_m = K_m^0 + K_{mj}^P \alpha_j^P \qquad (m = 1, \ldots, 2n,\ j = 1, \ldots, n)$$

Here K_m^0 is the stress intensity factor at crack tip m due to the remote tractions, and K_{mj}^P is the stress intensity factor at crack tip m due to the pressure in crack j.

We also require the pressure scaling values to be linearly dependent and thus can be expressed as $\alpha_j^P = \beta_j^P \alpha_n^P$. In the case of equal injection pressure in each crack, β_j is a vector of ones. We can then calculate the stress intensity factors due to a unit pressure in each crack, scale the stress intensity factors such that the SIF at each tip reaches the critical value, and then take the minimum pressure scaling value to causes the cracks to grow. We find the pressure in the n^{th} crack to be

$$\alpha_n^P = \min \left(\frac{\mathrm{K_{IC}} - \mathrm{K_m^0}}{\mathrm{K_{mj}^P} \beta_\mathrm{j}^\mathrm{P}} \right).$$

Thus we find the pressure in each crack necessary for crack growth to commence.

2.4.2 Linearly Dependent Injection Volumes

We also consider a strategy to simulate crack propagation due to linearly dependent injection volumes. The pressure scaling values, α_j^P, are now subject to the following stress intensity factor and volume constraints:

$$V_i = V_i^0 + V_{ij}^P \alpha_j^P \qquad (i, j = 1, \ldots, n)$$
$$K_m = K_m^0 + K_{mj}^P \alpha_j^P \qquad (m = 1, \ldots, 2n)$$

Here V_i^0 is the volume of crack i due to the remote tractions, V_{ij}^P is the volume of crack i due to the pressure in crack j, K_m^0 is the stress intensity factor at crack tip m due to the remote tractions, and K_{mj}^P is the stress intensity factor at crack tip m due to the pressure in crack j.

The volume in each crack can then be specified, and taken relative to the volume in the n^{th} crack, such that $V_i = \beta_i^V V_n$. As in the case of prescribed injection pressure, when β_i^V is a vector of ones, then all n cracks have equal volume. Considering the pressure in the n^{th} crack to be specified, we can rewrite our volume constraint as $n-1$ equations and unknowns

$$\left(V_{ij}^P - \beta_i^V V_{nj}^P\right) \alpha_j^P = \left(\beta_i^V V_n^0 - V_i^0\right) + \left(\beta_i^V V_{nn}^P - V_{in}^P\right) \alpha_n^P.$$

This system of equations is of the form

$$A_{ij} \alpha_j^P = L_i + M_i \alpha_n^P,$$

such that $A_{ij} = V_{ij}^P - \beta_i^V V_{nj}^P$, $L_i = \beta_i^V V_n^0 - V_i^0$, and $M_i = \beta_i^V V_{nn}^P - V_{in}^P$ are all known. We can then solve the two linear systems of equations

$$A_{ij} \alpha_j^L = L_i \text{ and } A_{ij} \alpha_j^M = M_i.$$

Our pressure solution for our original equation is

$$\alpha_j^P = \alpha_j^L + \alpha_j^M \alpha_n^P.$$

Our last remaining unknown is α_n^P, which we can solve for using the SIF constraint. Substituting our pressure solution into the SIF constraint yields

$$K_m = K_m^0 + K_{mj}^P \left(\alpha_j^L + \alpha_j^M \alpha_n^P\right).$$

Solving for each of the m crack tips, we have

$$\alpha_n^P(m) = \frac{K_{IC} - K_m^0 - K_{mj}^P \alpha_j^L}{K_{mj}^P \alpha_j^M}.$$

We choose the smallest α_n^P, as this will give us the smallest pressure necessary to initial crack growth. From this pressure solution we can calculate the total tractions, opening displacements, and SIF's for the given load step. We can then calculate the growth of crack crack for the given load step from these stress intensity factors.

CHAPTER 3
RESULTS

3.1 Analytic Solutions and Verification of Results

Towards verifying that our computational model is valid, we can compare the results of several simple crack geometries to well known analytic solutions.

3.1.1 Two Parallel Cracks

We first consider the case of two parallel cracks of length $2a$, separated by distance d, and subject to uniform remote tension, σ_0 as shown in Figure 3.1. Murakami's SIF Handbook utilizes a continuous distribution of infinitesimal dislocations to derive that stress intensity factors at the crack tips (Murakami 1987).

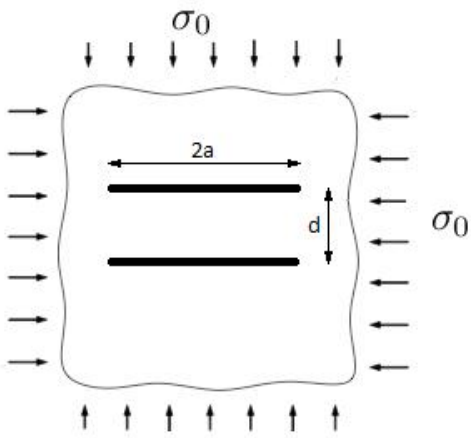

Figure 3.1: Crack Geometry and Remote Loading for Two Parallel Cracks

From Murakami's solution, the SIF at each tip is given by

$$K_I = F_I \sigma_0 \sqrt{\pi a}$$

with

$$F_I = 1 - 0.0007\lambda - 0.4130\lambda^2 + 0.2687\lambda^3$$

and

$$\lambda = \frac{2a}{d}.$$

Considering the case in which $\lambda = \frac{2}{3}$ we find $K_I = 2.2449\sigma_0$. Solving for the SIF's using HyFrac2D, we find $K_I = 2.2467\sigma_0$, which is a difference of 0.08%.

3.1.2 Three Parallel Cracks

Murakami's SIF Handbook utilizes a Laurent series expansion solution to derive the stress intensity factors at the tips of three parallel cracks of length $2a$, separated by distance d, under uniform remote tension σ_0 as shown in Figure 3.2.

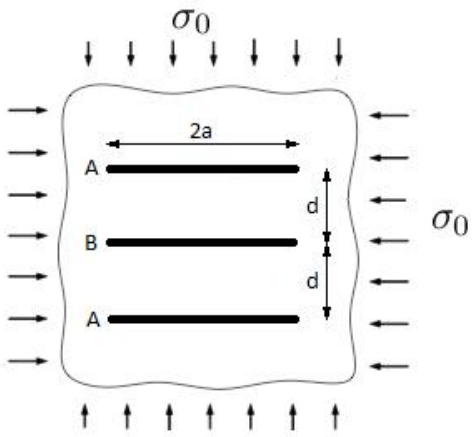

Figure 3.2: Crack Geometry and Remote Loading for Three Parallel Cracks

The SIF at each tip is now given by

$$K_I = F_I \sigma_0 \sqrt{\pi a}$$

with

$$\lambda = \frac{2a}{d}$$

but with F_I given by a chart in the SIF Handbook. Taking $\lambda = \frac{4}{3}$, we find that

$$\begin{aligned} F_{IA} &= 0.78 \quad \text{and} \quad F_{IB} = 0.64 \\ K_{IA} &= 1.955\sigma_0 \quad \text{and} \quad K_{IB} = 1.604\sigma_0. \end{aligned}$$

HyFrac computes $K_{IA} = 1.9584\sigma_0$ and $K_{IB} = 1.5831\sigma_0$, a difference of 0.17% and 1.3%, respectively.

3.2 Opening Displacements

The growth of the three parallel cracks is initially counter-intuitive. The tips of the outer cracks initially have larger stress intensity factors than the middle crack, meaning that they will grow first. Indeed the outer crack tips eventually come to dominate growth and by 500 load steps are much longer than the middle crack. Consider first the case of three cracks with equal volumes. Given equal volume, but a shorter length, the middle crack would be expected to have a larger crack opening displacement. This would indicate that the middle crack should have large SIFs. This is however, not the case. Rather, the two outer cracks constrict at the center and have their largest openings near the tips. This contributes to larger SIFs at the tips of the outer cracks. This is consistent with the stress from the outer cracks "closing" the middle crack, and the stress from the middle crack "closing" the center of the outer cracks once the tips have grown significantly.

This effect is even more dramatic for the case of equal injection pressures. The stress intensity factor is proportional to the stress and to the square root of the crack length. Therefore for a given pressure, a longer crack will have a larger stress intensity factor. The result of this is that the middle crack does not grow at all, as the internal pressure is never large enough to overcome the compressive stresses of the remote loading and the outer cracks.

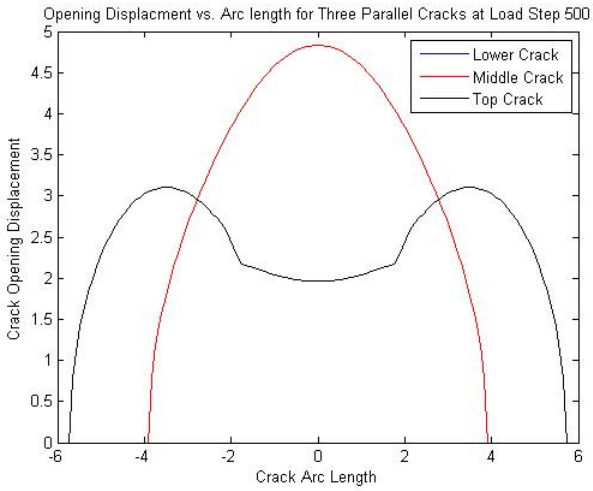

Figure 3.3: Opening Displacements for Three Parallel Cracks with Equal Injection Volumes

3.3 Pressure and Volume Constraints

We now investigate the growth vertically aligned and offset parallel cracks subject to either the constraint of equal injection volumes or equal injection pressures. Though the number of crack geometry that HyFrac2D can predict crack growth for is only restricted to non-intersecting cracks, we consider only the case of vertically offset parallel cracks, with the geometry for three cracks shown in the Figure 3.4. In the following cases we take $\frac{2a}{d} = \frac{4}{3}$. For vertically aligned cracks we set, $b = 0$, and in the case of offset cracks we let $2a = b$.

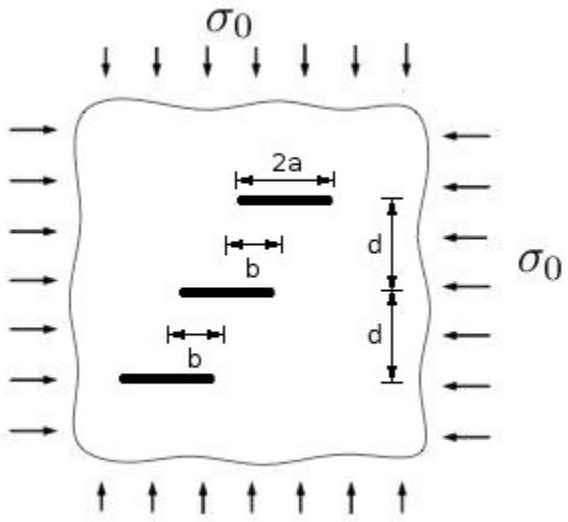

Figure 3.4: Crack Geometry and Remote Loading for Three Offset Cracks

3.3.1 Vertically Aligned Parallel Cracks

We now consider vertically aligned parallel cracks subject to equal injection volume and equal injection pressure. For the crack of two parallel cracks, we find that both cases yield identical results, as can be seen in Figure 3.5. As discussed previously, the stress intensity factors at each crack tip are equal. Because of the symmetry of the problem, this means that the opening displacements, and subsequently the volumes, of each crack must be equal. It then follows that the injection pressures must also be equal. This holds true at every load step and thus the crack growth for either equal injection volumes or pressures is identical.

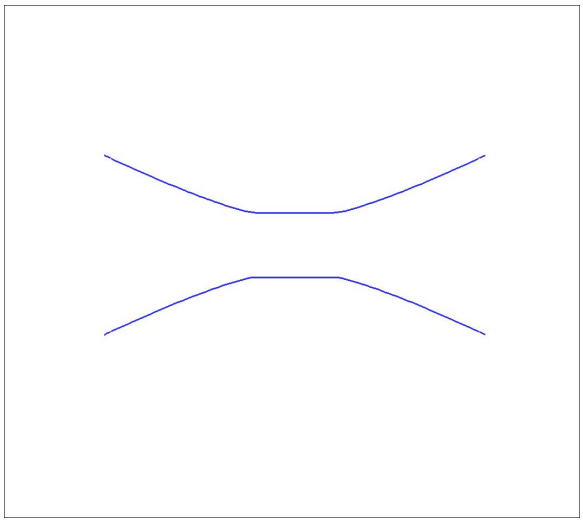

Figure 3.5: Identical Crack Growth for 2 Aligned Cracks
with Equal Injection Pressures and Volumes

Because the stress intensity factor is proportional to the remote loading and to the square root of the crack length, it follows that as the cracks grow, the internal pressure necessary to propagate those cracks decreases.

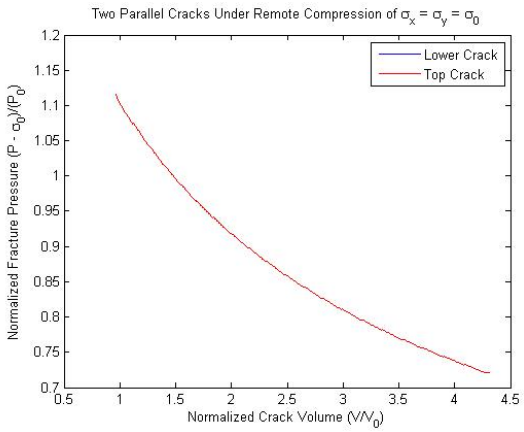

Figure 3.6: Fracture Pressure for Two Parallel Cracks

We also observe that for both cracks the normalized injection volume and normalized crack length remain identical at each load step.

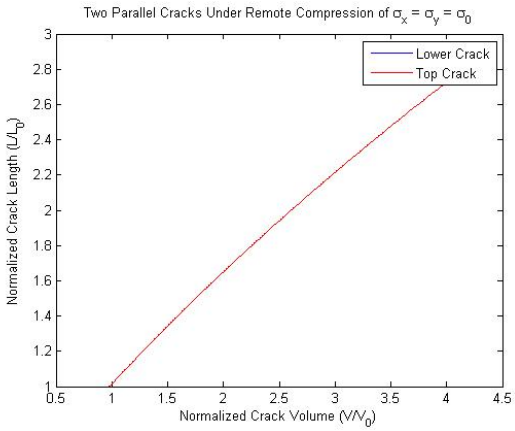

Figure 3.7: Crack Length for Two Parallel Cracks

The pressures and volumes are normalized relative to the analytic solution for fracture pressure and volume of a single pressurized crack of length a. These reference pressures and volumes are given by

$$P_0 = \frac{K_{IC}}{\sqrt{\pi a}} \qquad \text{and} \qquad V_0 = \frac{(1-\nu)}{\mu}\pi P_0 a^2.$$

Turning our attention to three vertically aligned parallel cracks, we find that the crack growth is no longer identical. As shown in the previous discussion of crack opening displacements, the middle crack does not grow at all for the case of equal injection pressures, and grows far less than the outer cracks for the case of equal injections volumes. The remote stresses produced by the opening displacements of the middle crack tend to drive the outer cracks away from the horizontal (and thus away from the middle crack). Because the middle crack grows in volume constraint case, the larger remote stresses cause the outer cracks to turn more than for the pressure constraint case as shown in Figure 3.8. It should be noted that, because we use a specified maximum growth length for each load step, at any given load step the outer cracks are of equal length for the pressure and volume constraint cases.

As in the two crack case, for three cracks with equal injection volumes, the internal pressure necessary to propagate the cracks decreases as the crack length increases.This effect can be seen in the following figure. This further illuminates why, for the case of equal

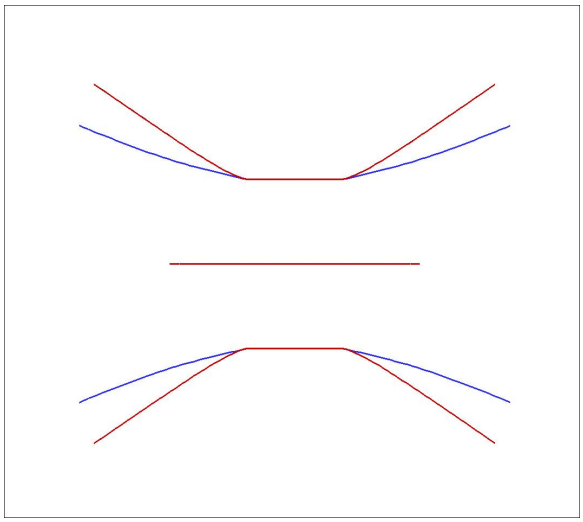

Figure 3.8: Crack Growth for 3 Aligned Cracks
with Equal Injection Pressures (Blue) and Volumes (Red)

injection pressures, the middle crack does not grow. The middle crack requires a larger internal pressure in order to grow. In the case of equal volume injections, the middle crack does indeed reach the pressure necessary to grow the crack. In the case of equal injection volumes, the outer cracks reach K_{IC} first, and additional growth only drives down the required pressure, ensuring that the middle crack will never grow.

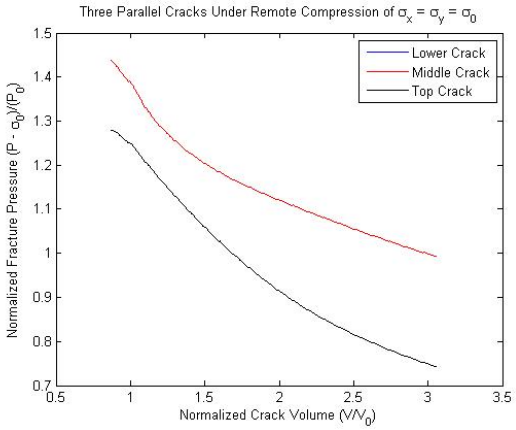

Figure 3.9: Fracture Pressure for Three Parallel Cracks

For the three crack case with equal injection volumes, we find that the initial crack growth for all cracks is nearly linear with respect to normalized crack volume. As the cracks grow, and the opening displacements take on the behavior discussed earlier, the outer cracks continue to grow nearly linearly, while growth of the middle crack slows.

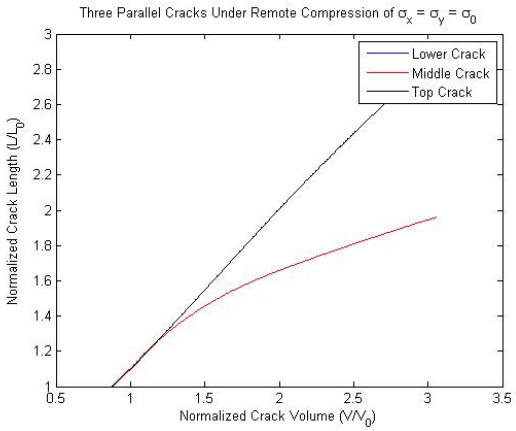

Figure 3.10: Crack Length for Three Parallel Cracks

Considering more than three vertically aligned parallel cracks, we see that the behavior shown for three aligned cracks continues. For the case of equal injection pressures, only the outer cracks grow. The tips of the outer cracks reach K_{IC} first, as then have less confining stress, and thus grow first. As soon as these outer cracks are longer than the interior cracks, it takes even less pressure to grow them. Thus as load steps increase, the internal pressure drops, and while the outer cracks continue to grow, the stress intensity factors for the tips of the interior cracks decrease monotonically. The relatively small stresses from these interior cracks, result in outer cracks that do not turn away from the horizontal very much. For the case of equal injection volumes, the increasing volumes in the interior cracks do cause the interior cracks to grow somewhat. This causes the outer cracks to turn more dramatically away from the horizontal. As the outer cracks turn away from the horizontal, the reduction in confining stress further from the x-axis also drives the interior cracks away from the horizontal, though less dramatically. This can be seem in Figures 3.11 and 3.12 for four

aligned cracks and seven aligned cracks, respectively. It should be noted that this behavior is also present in the cases of five and six aligned cracks.

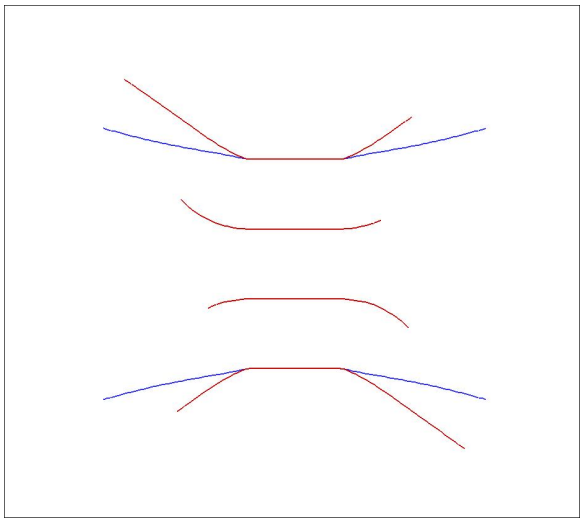

Figure 3.11: Crack Growth for 4 Aligned Cracks
with Equal Injection Pressures (Blue) and Volumes (Red)

For the case of equal injection volumes, we observe the beginnings of what we will term "anti-symmetric" behavior, which is to say small perturbations seem to eventually drive adjacent cracks in opposite directions. This effect will be discussed in greater detail in section 3.4.

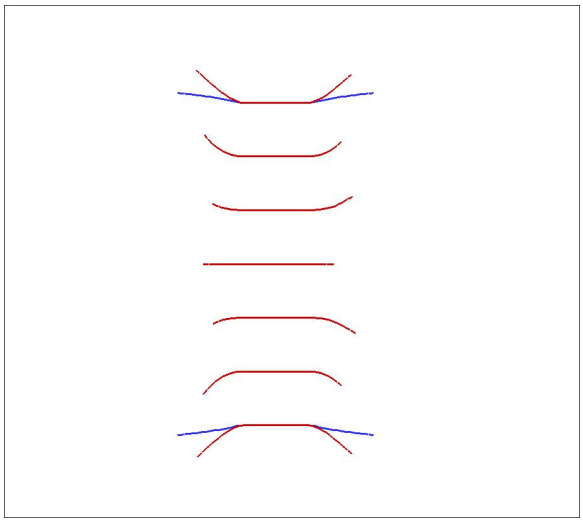

Figure 3.12: Crack Growth for 7 Aligned Cracks
with Equal Injection Pressures (Blue) and Volumes (Red)

3.3.2 Vertically Offset Parallel Cracks

Next, consider vertically offset parallel cracks subject to equal injection volume and equal injection pressure. As in the case of two aligned cracks, both cases yield identical results, as can be seen in Figure 3.13. As discussed previously, the stress intensity factors at each crack tip, and thus the injection volumes and pressures of each crack must be equal. In this case, the outer tips of both cracks slowly turn away from the horizontal, behavior that has previously been explained as reducing the compressive stress from the other crack. The inner crack tips however, turn towards each other and begin to "spiral" inwards. The additional compressive stress from the other crack causes a positive (in the local crack tip coordinate system) mode-II SIF and thus induces each crack to turn towards each other.

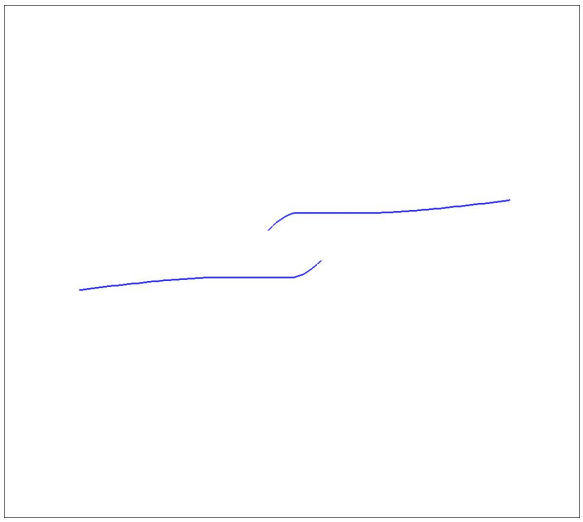

Figure 3.13: Identical Crack Growth for 2 Offset Cracks
with Equal Injection Pressures (Blue) and Volumes (Red)

For three offset parallel cracks, the behavior observed for two offset cracks continues. The outer tips of the outer cracks turn away from the horizontal, while the inner tips of all three cracks begin to "spiral" inward. As in the case of three aligned cracks, three offset cracks have different behavior for both equal injection volumes and pressures. Interestingly, the middle cracks do grow for both the volume and pressure constraint cases.

Equal Injection Pressure

Crack	L/L_0	V/V_0	$(P-\sigma_0)/P_0$
Lower	9.0298	3.7088	0.4666
Middle	10.6459	5.3172	0.4666
Upper	9.0298	3.7088	0.4666

Equal Injection Volume

Crack	L/L_0	V/V_0	$(P-\sigma_0)/P_0$
Lower	11.3989	5.3936	0.4157
Middle	10.1896	5.3936	0.4711
Upper	11.3989	5.3936	0.4157

Table 3.1: Length, Volume, and Pressure Data for Three Offset Cracks

Comparing the normalized crack lengths, pressures, and volumes for each constraint at load step 900 as listed in Table 3.1. For equal injection pressures, we find that the middle

crack in fact grows slightly more than the outer cracks. For equal injection volumes however, the outer cracks grow slightly more than the middle crack. Additionally, the outer cracks turn more for the equal injection pressure case, while the middle crack turns more for the equal injection volume case. The behavior observed in the case of three offset cracks also occurs in the case of four offset parallel cracks.

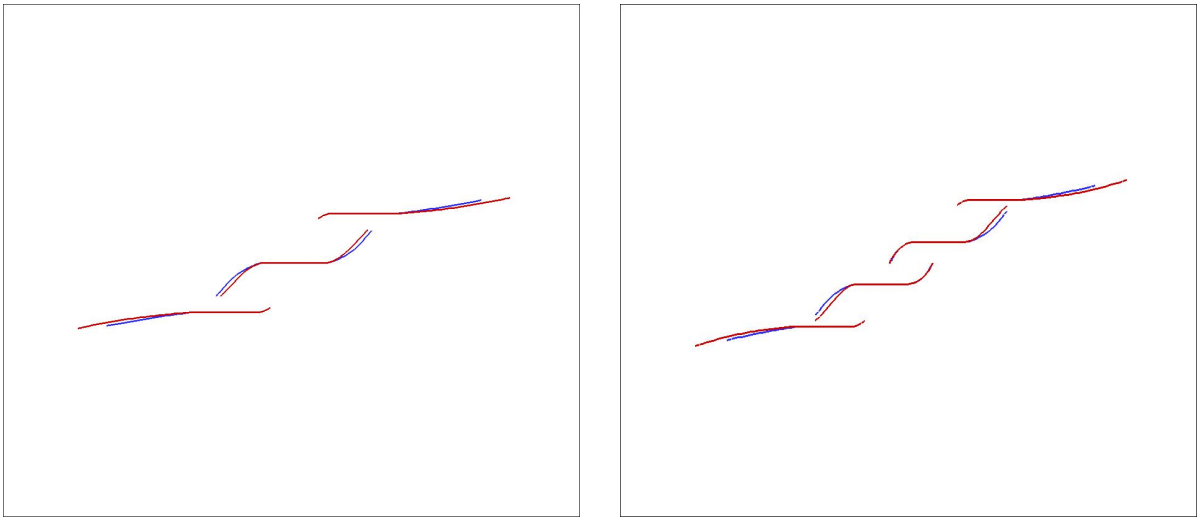

Figure 3.14: Crack Growth for both 3 and 4 Offset Cracks
with Equal Injection Pressures (Blue) and Volumes (Red)

3.4 Anti-Symmetric Growth of Aligned Cracks

For the previously discussed cases of equal volume injections, we remarked that with four or more aligned cracks, an "anti-symmetric growth" behavior developed. To investigate this behavior further, we now consider vertically aligned cracks that are closer together, such that $\frac{2a}{d} = 2$, which increases the interaction of the cracks, and increases this anti-symmetric behavior as seen in Figure 3.15.

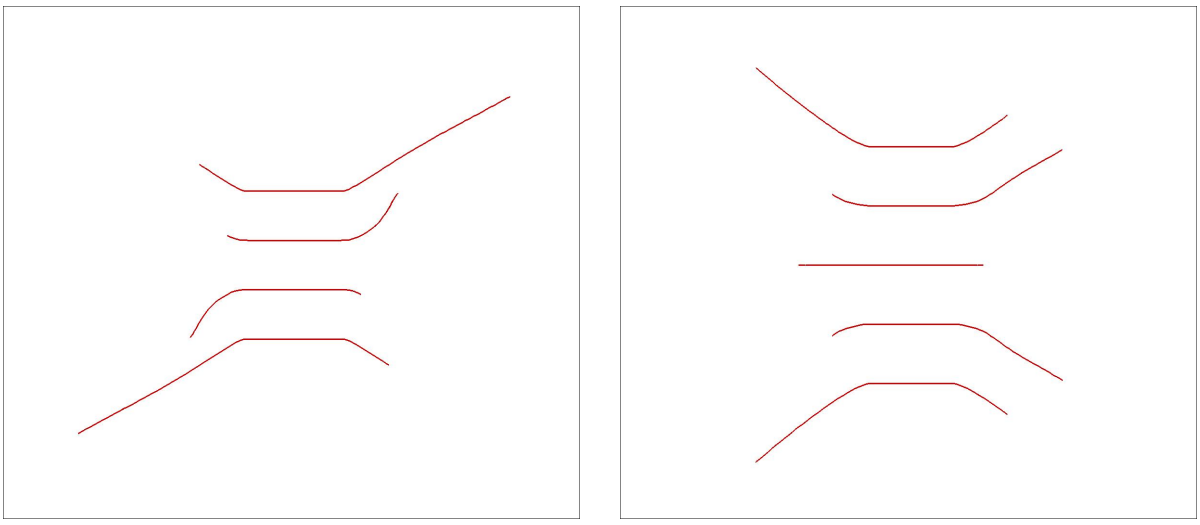

Figure 3.15: Antisymmetric Crack Growth for 4 and 5 Aligned Cracks

It would seem that small perturbations eventually cause one tip of a given crack to grow more than the other tip. Table 3.2 gives the Stress Intensity Factors at each crack tip for 4 parallel cracks at load steps 1, 160, 300, and 500. Nodes 1 and 17 are the tips of crack 1 (the top crack), nodes 18 and 34 are on crack 2, nodes 35 and 51 are on crack 3, and nodes 52 and 68 are on crack 4 (the bottom crack). The SIF's of each crack initially start out symmetric and for this case retain symmetry until load step 160 at which point the "antisymmetry" begins very subtly at the fifth decimal place. This small perturbation is sufficient to cause the growth of the crack tip with larger SIF on each crack to begin to dominate the growth. This trend continues until the shorter crack tips growth has halted, as can be seen in the smaller SIF's of load step 300 and 500, while the other tip on any given crack continues to grow. This effect does not seem to be solely attributable to round off error, as the grow still remains "antisymmetric", with opposite crack tips on corresponding cracks across the x-axis having identical SIF's, and identical lengths, pressures, and volumes of the corresponding cracks. Additionally, changing the nodal numbering of the cracks, such that their information is stored at a different location in the stiffness matrix does not change the behavior, and at most flips the symmetry of the cracks across the y-axis.

SIF's at Load Step 1

Node	KI	KII
1	0.9370479	0.2226634
17	0.9370479	0.2226634
18	1.0000000	0.0606462
34	1.0000000	0.0606462
35	1.0000000	-0.0606462
51	1.0000000	-0.0606462
52	0.9370479	-0.2226634
68	0.9370479	-0.2226634

SIF's at Load Step 160

Node	KI	KII
1	1.0000000	0.0003035
17	0.9999999	0.0003031
18	0.9649220	0.0122301
34	0.9649019	0.0122359
35	0.9649019	-0.0122359
51	0.9649220	-0.0122301
52	0.9999999	-0.0003031
68	1.0000000	-0.0003035

SIF's at Load Step 300

Node	KI	KII
1	1.0000000	-0.0005261
17	0.9142912	0.0024639
18	0.9768593	0.0059224
34	0.7542543	0.0123228
35	0.7542543	-0.0123227
51	0.9768593	-0.0059224
52	0.9142912	-0.0024639
68	1.0000000	0.0005261

SIF's at Load Step 500

Node	KI	KII
1	1.0000000	-0.0004967
17	0.6270734	0.0235751
18	0.9650601	0.0063857
34	0.6050907	-0.0659453
35	0.6050907	0.0659453
51	0.9650601	-0.0063857
52	0.6270734	-0.0235751
68	1.0000000	0.0004967

Table 3.2: SIF's for 4 aligned parallel cracks

As can be seen in Figures 3.15 and 3.16, geometries with an even number of cracks cracks show slightly different "antisymmetric" behavior than geometries with an odd number of cracks. The growth of an odd number of cracks seems to be symmetric across the x-axis, while the growth of an even number of cracks seems to be rotationally symmetric about the

origin. For an odd number of cracks, when one tip begins to grow, the adjacent cracks are subject to an increased confining stress that limits their growth, thus reducing the confining stress on the crack tips of any adjacent cracks, allowing those tips to grow. Once this pattern begins, we observe the alternating growth - no growth behavior of adjacent crack tips. Because we have an odd number of tips, if one tip of the top crack dominates growth, the mirror image across the x-axis will occur for the growth of the bottom crack. This produces the observed symmetry across the x-axis. The behavior for even number of cracks is not quite as easily explained. For the case of four cracks, while the SIF's remain symmetric, the outer cracks dominate the growth. Once the anti-symmetry presents itself, the middle cracks tend to "follow" the outer cracks, as seen 3.15. For the case of six parallel cracks, while the SIF's are symmetric, the outer cracks dominate growth. Once the asymmetry begins however, the two inner-most cracks begin to dominate the growth, with the opposite tips growing from the crack tips that grew on the outer tip. Both these situations lead to the rotational symmetry of the growth of an even number of cracks.

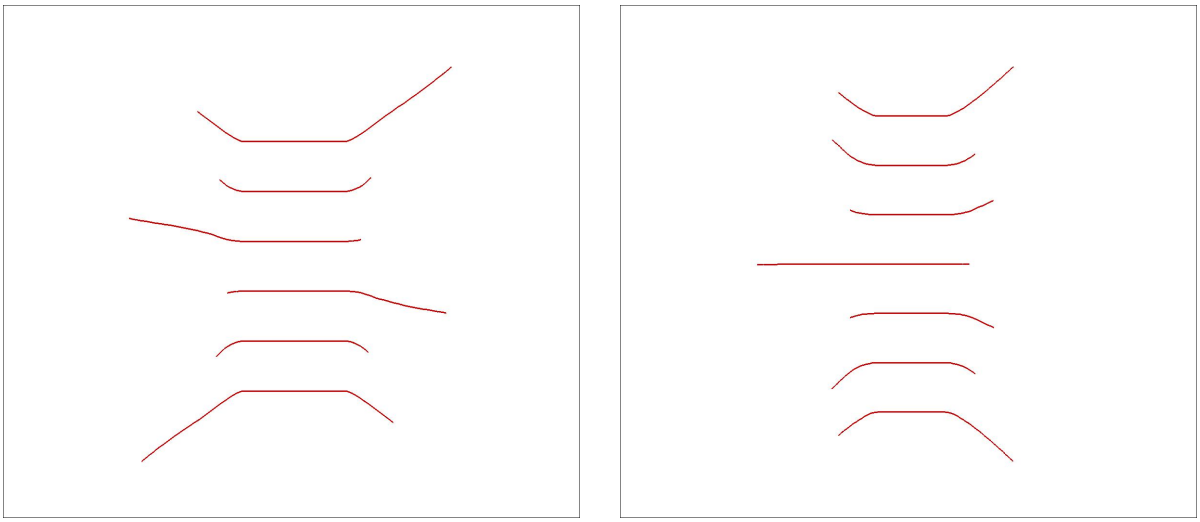

Figure 3.16: Antisymmetric Crack Growth for both 6 and 7 Aligned Cracks

CHAPTER 4
CONCLUSIONS

This paper presented a computational procedure utilizing a symmetric Galerkin boundary element method (SGBEM), based on a weakly singular, weak-form traction integral equation to model fractures in isotropic linearly elastic media. Multiple interacting cracks in an unbounded domain subject to internal pressure and remote stress were considered. first, it was found that the stress intensity solutions closely matched analytic solutions for simple crack geometries. We then investigated the differing growth of cracks subjected to either equal injection pressures or equal injection volumes. The different crack growth behavior for each case was explained in terms of the stresses in the domain produced by the pressure in each crack and subsequently, each cracks effect on its neighboring cracks. It was found that, for our simple model of an inviscid fluid, the volume constraint seemed to display more interesting behavior, which is to say, all the cracks grew, while for the pressure constraint, the outer cracks dominated growth. Finally the antisymmetric behavior of large numbers of cracks was presented. This antisymmetric behavior appears to be the greatest area for further research, particularly in the context of hydraulic fracturing, as a single well-bore may have many fractures originating from it.

The current version of the HyFrac2D code has several limitations and thus opportunity for future work to improve the model of multiple interacting cracks. Currently the constant internal pressure is a very simple model for fluid in the crack, corresponding to the case of an inviscid fluid. Towards improving the model's response to fluid flow in the crack, the next major step would be to model fluid in the crack using finite elements. This would utilize a coupled SGBEM-FEM formulation that has already be derived and implemented for three dimensions, and could be reduced to two dimensions for implementation in HyFrac2D.

There is also a simplification in the way that the code calculates $\bar{K}_I$ and equates it to K_{IC}. In section 2.3 we defined the equivalent mode-I SIF to be

$$\bar{K}_I = K_I \cos^3\left(\frac{\theta_g}{2}\right) - \frac{3}{2} K_{II} \cos\left(\frac{\theta_g}{2}\right) \sin\theta_g,$$

with the growth direction given by

$$\tan\left(\frac{\theta_g}{2}\right) = \frac{K_I - \sqrt{K_I^2 + 8K_{II}^2}}{4K_{II}}, \qquad -\pi \leq \theta_g \leq \pi$$

and the SIF's at crack tip m given by

$$K_m = K_m^0 + K_{mj}^P \alpha_j^P.$$

Thus we can write the growth angle in terms of the SIF's due to the remote stress and the pressures in each crack as

$$\tan\left(\frac{\theta_g}{2}\right) = \frac{1}{4}\left[\frac{K_I^0 + K_I^j \alpha_j}{K_{II}^0 + K_{II}^j \alpha_j} - \sqrt{8 + \left(\frac{K_I^0 + K_I^j \alpha_j}{K_{II}^0 + K_{II}^j \alpha_j}\right)^2}\right].$$

The presence of the remote stress SIF's mean that the growth angle is not a linear function of the SIF's and thus we do not know the growth angle until we compute the pressure scaling values. This means $\bar{K}_I$ cannot be computed a priori for each crack tip, nor can they be compared to K_{IC} to calculate the pressure scaling values and thus cannot be used to compute the amount that each tip will grow.

To get around this complication, we instead set $K_I = K_{IC}$ for the crack tip with the largest mode-I SIF, and scale the other cracks according to the ratio of their mode-I SIF to K_{IC}. Let us consider two crack tips, with larger SIF's at the first crack tip such that the first crack tip will grow more than the second. For the first crack tip, we have

$$\frac{\bar{K}_I^{(1)}}{\bar{K}_{\max}} = \frac{\bar{K}_I^{(1)}}{\bar{K}_I^{(1)}} = \frac{K_I^{(1)}}{K_{IC}} = 1$$

and thus the crack tip growth the maximum amount whether we set K_I or $\bar{K}_I$ equal to K_{IC}. However for the second crack tip, we have

$$\frac{\bar{K}_I^{(2)}}{\bar{K}_{\max}} = \frac{\bar{K}_I^{(2)}}{\bar{K}_I^{(1)}} \neq \frac{K_I^{(2)}}{K_{IC}}$$

and therefore other crack tips do not grow the same amount with our simplification as they should in the real formulation. Additionally, the growth angles for all the cracks will not be identical in both formulations. The question is how much does this affect the crack growth behavior? When there is no remote stress, the two strategies are identical. Thus when the remote stress is small relative to the stresses produced by the pressures in crack, the effect on the crack growth behavior should also be small. It is thus left as an area of possible future work to correctly equate the equivalent mode-I stress intensity factor to the critical SIF.

REFERENCES

Han D. Tran and M.E. Mear (2010). *FADD2D User's Manual*. Dept. of Aerospace Engineering and Engineering Mechanics. The University of Texas at Austin.

Murakami, Y. (Ed.) (1987). *Stress Intensity Factor Handbook*, Volume I. Oxford: Pergamon Press.

Tran, H. D. (2010). *A Computational Procedure for Analysis of Fractures in Two-dimensional Multi-field Media*. Ph. D. thesis, The University of Texas at Austin.

VITA

Andrew Erickson was born in Kirkland, Washington. He attended Whitman College and received the degree of Bachelor of Arts in May 2009. In Austin 2010 he entered the Graduate School at The University of Texas at Austin as a student in the Aerospace Engineering and Engineering Mechanics department.

Permanent Email Address: andrew.erickson26@gmail.com

This report was typed by the author.